New Journal of Physics
The open access journal at the forefront of physics

Deutsche Physikalische Gesellschaft DPG IOP Institute of Physics

PAPER • OPEN ACCESS

Galvanically connected tunable coupler between a cavity and a waveguide

To cite this article: Kazuki Koshino 2025 *New J. Phys.* **27** 043001

IOP Publishing New J. Phys. 27 (2025) 043001 https://doi.org/10.1088/1367-2630/adc1fb

New Journal of Physics
The open access journal at the forefront of physics

Deutsche Physikalische Gesellschaft DPG
IOP Institute of Physics

Published in partnership with: Deutsche Physikalische Gesellschaft and the Institute of Physics

OPEN ACCESS

RECEIVED
30 December 2024

REVISED
5 March 2025

ACCEPTED FOR PUBLICATION
18 March 2025

PUBLISHED
31 March 2025

PAPER

Galvanically connected tunable coupler between a cavity and a waveguide

Kazuki Koshino

Institute for Liberal Arts, Institute of Science Tokyo, 2-8-30 Konodai, Ichikawa, Chiba 272-0827, Japan

E-mail: kazuki.koshino@osamember.org

Keywords: tunable coupler, waveguide QED, circuit QED, superconducting device, stub filter

Abstract

One of the key technologies in recent quantum devices is the tunable coupling between quantum elements such as qubits, cavities, and waveguides. In this work, we propose a cavity-waveguide tunable coupler realized in a semi-infinite waveguide equipped with a tunable stub. The working principle of the present device is the shift of the node position of the cavity mode induced by the tunable boundary condition at the stub end, and the advantage of the present device is an extremely wide tunability of the cavity-waveguide coupling. When the node position is adjusted to the branch point of the waveguide, the cavity mode becomes decoupled from the waveguide modes in principle. At the same time, owing to the galvanic connection, the present device readily achieves an ultrastrong cavity-waveguide coupling, where the cavity decay rate reaches the order of a gigahertz, comparable to the cavity resonance frequency.

1. Introduction

Regardless of their physical implementation, cavity quantum electrodynamics (QED) systems are commonly characterized by only a few parameters, such as the resonance frequencies of the atom and the cavity (ω_a, ω_c), their mutual coupling rate (g), and their decay rates (γ, κ) [1, 2]. One of the appeals of cavity QED systems lies in their high designability. We can artificially set the cavity-related parameters (ω_c, g, and κ) through the design of the cavity. In solid-state cavity QED systems using artificial atoms, the atom frequency ω_a also becomes a designable parameter and an unprecedentedly strong atom-cavity coupling g becomes in reach [3, 4].

Cavity QED systems acquire further flexibility by the possibility of *in-situ* tuning of system parameters through the external fields. In circuit QED, a superconducting quantum interference device (SQUID) is used as a tunable element through the magnetic flux threading the loop [5]. For example, by replacing a Josephson junction composing a qubit with a SQUID, *in-situ* tuning of the qubit frequency becomes possible [6–8]. Such a frequency-tunable qubit is applicable to a tunable coupler between two qubits [9], which is indispensable to achieve a high two-qubit gate fidelity. Tunable couplers now play an essential role in constructing various quantum devices. Besides the qubit–qubit coupling [9–15], tunable coupling has been developed in the cavity–cavity coupling [16–18], the qubit-waveguide coupling [19–22], and the cavity-waveguide coupling [23–27].

In this study, we propose a cavity-waveguide tunable coupler whose working principle differs fundamentally from the conventional tunable couplers. The proposed setup is a semi-infinite transmission line equipped with a tunable stub [figure 1(a)], where the two finite ports (one infinite port) function as a cavity (waveguide). The cavity-waveguide coupling is tuned through the shift of the node position of the cavity mode. The cavity mode becomes completely decoupled from the waveguide modes in principle when its node position is adjusted to the branch point of the waveguide. In contrast, due to the galvanic connection, the cavity-waveguide coupling readily reaches the ultrastrong coupling regime, where the cavity decay rate amounts to the order of gigahertz, comparable to the resonance frequency.

The rest of this paper is organized as follows. In section 2, we present the setup investigated in this work, namely, a semi-infinite waveguide equipped with a tunable stub. In section 3, we analyze the continuous

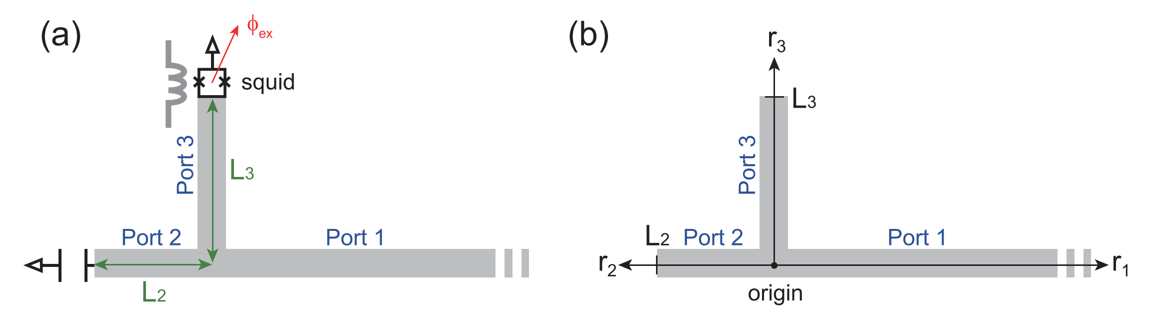

Figure 1. (a) Schematic of the investigated setup. The external magnetic flux threading the SQUID loop, $\Phi_{\text{ex}} = (\hbar/2e)\phi_{\text{ex}}$, is controlled by a DC current near the loop. (b) Coordinate system employed in this work.

Table 1. List of parameters. C_s and E_s are the values for the two identical Josephson junctions forming the SQUID.

v	(microwave velocity)	$10^8\,\text{m}\,\text{s}^{-1}$
Z	(characteristic impedance)	$50\,\Omega$
L_2	(length of Port 2)	2.5 mm
L_3	(length of Port 3)	4.5 mm
C_s	(capacitance)	100 fF
$(2e/\hbar)E_s$	(critical current)	$5\,\mu$A

eigenmodes of this waveguide. We observe the existence of a discrete cavity mode, which is decoupled from the propagating modes in the semi-infinite part of this waveguide, under a proper boundary condition at the stub end. In section 4, we analyze the microwave response of the cavity mode to the stationary field input from the semi-infinite part. We focus on the phase shift of the input field upon reflection and the photon energy stored in the cavity. From the results of microwave response, we determine in section 5 the resonance frequency and the linewidth of the cavity. We observe that the linewidth is extremely sensitive to the boundary condition at the stub end and therefore that the cavity-waveguide coupling is widely tunable from the complete decoupling to the ultrastrong coupling of the order of gigahertz. We summarize this work in section 7.

2. Setup

In this study, we investigate a waveguide composed of three ports with the same properties (characteristic impedance Z and microwave phase velocity v), as illustrated schematically in figure 1(a). Port 1 is semi-infinite, whereas Ports 2 and 3 have finite lengths of L_2 and L_3, respectively. Port 2 is terminated by an infinitesimal capacitance to the ground and the boundary condition there is open for the voltage. Port 3 is terminated by a SQUID so as to enable *in-situ* tuning of the boundary condition by the external magnetic flux threading the loop. Setting the origin at the waveguide branch, we take a coordinate system depicted in figure 1(b). For concreteness, we employ the parameter values listed in table 1.

3. Eigenmodes

In this section, we investigate the eigenmodes of this waveguide. As a variable to describe the microwave propagating in this waveguide, we employ the flux (time-integrated voltage) defined by $\phi(r,t) = \int^t \mathrm{d}t' V(r,t')$. Considering the semi-infinite nature of this waveguide, its eigenmodes are labelled by a continuous frequency $\omega(>0)$. The eigenmode function at frequency ω is written, denoting its amplitude in Port $j(=1,2,3)$ by $\alpha_\omega^{(j)}$ and the phase of the standing wave in Port 1 by θ_ω, as

$$\phi_\omega(r) = \begin{cases} \phi_\omega^{(1)}(r_1) = \alpha_\omega^{(1)} \cos(\omega r_1/v + \theta_\omega) & \text{(Port 1)} \\ \phi_\omega^{(2)}(r_2) = \alpha_\omega^{(2)} \cos[\omega(r_2 - L_2)/v] & \text{(Port 2)} \\ \phi_\omega^{(3)}(r_3) = \alpha_\omega^{(3)} \cos\left[\omega\left(r_3 - L_{3,\omega}^{\text{eff}}\right)/v\right] & \text{(Port 3)} \end{cases}, \tag{1}$$

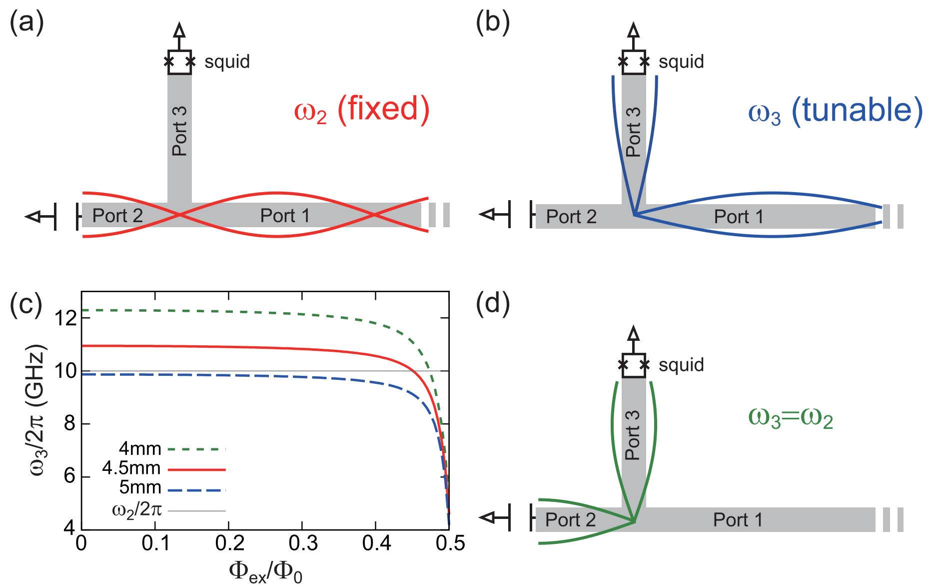

Figure 2. Eigenmode having a node at the waveguide branch. (a) Eigenmode with vanishing amplitude in Port 3. Its eigenfrequency is denoted by ω_2. (b) Eigenmode with vanishing amplitude in Port 2. Its eigenfrequency is denoted by ω_3. (c) Tuning of ω_3 through the boundary condition. Φ_{ex} is the magnetic flux threading the SQUID loop and $\Phi_0 (= h/2e)$ is the flux quantum. Thin line plots ω_2, which is fixed at $2\pi \times 10$ GHz. (d) Cavity mode, the amplitude of which vanishes in Port 1. This mode appears under a specific boundary condition, where $\omega_3 = \omega_2$. Note that the frequency of this mode is determined solely by the length of Port 2 [equation (6)].

where $L^{\mathrm{eff}}_{3,\omega}$ is the effective length of Port 3, which is tunable through the magnetic flux threading the SQUID (see appendix A). θ_ω and the ratio of $\{\alpha^{(1)}_\omega, \alpha^{(2)}_\omega, \alpha^{(3)}_\omega\}$ are determined by the following boundary conditions at the waveguide branch (see appendix B),

$$\phi^{(1)}_\omega(0) = \phi^{(2)}_\omega(0) = \phi^{(3)}_\omega(0), \tag{2}$$

$$\frac{\mathrm{d}\phi^{(1)}_\omega}{\mathrm{d}r_1}(0) + \frac{\mathrm{d}\phi^{(2)}_\omega}{\mathrm{d}r_2}(0) + \frac{\mathrm{d}\phi^{(3)}_\omega}{\mathrm{d}r_3}(0) = 0. \tag{3}$$

Equations (2) and (3) respectively represent the uniqueness of the voltage and the Kirchhoff's current law. From equations (1)–(3), we have

$$\alpha^{(1)}_\omega \cos\theta_\omega = \alpha^{(2)}_\omega \cos(L_2\omega/v) = \alpha^{(3)}_\omega \cos\left(L^{\mathrm{eff}}_{3,\omega}\omega/v\right), \tag{4}$$

$$\alpha^{(1)}_\omega \sin\theta_\omega = \alpha^{(2)}_\omega \sin(L_2\omega/v) + \alpha^{(3)}_\omega \sin\left(L^{\mathrm{eff}}_{3,\omega}\omega/v\right). \tag{5}$$

3.1. Special eigenmodes

First, we consider the eigenmodes whose amplitudes vanish in Port 3. Putting $\alpha^{(3)}_\omega = 0$ in equation (4), we observe that the eigenfrequencies of such modes satisfy $\cos(\omega L_2/v) = 0$. Hereafter, we focus on the lowest eigenmode satisfying this condition. We define the frequency ω_2 by

$$\omega_2 L_2/v = \pi/2. \tag{6}$$

At this frequency, we can confirm that $\alpha^{(1)}_{\omega_2} = \alpha^{(2)}_{\omega_2}$, $\alpha^{(3)}_{\omega_2} = 0$, and $\theta_{\omega_2} = \pi/2$. The spatial profile of this mode is schematically illustrated in figure 2(a). Similarly, we consider the lowest eigenmode whose amplitude vanishes in Port 2. The eigenfrequency ω_3 of this mode is determined by

$$\omega_3 L^{\mathrm{eff}}_{3,\omega_3}/v = \pi/2. \tag{7}$$

Regarding this mode, we have $\alpha^{(1)}_{\omega_3} = \alpha^{(3)}_{\omega_3}$, $\alpha^{(2)}_{\omega_3} = 0$, and $\theta_{\omega_3} = \pi/2$. The spatial profile of this mode is schematically illustrated in figure 2(b).

Note that ω_2 is a fixed value ($\omega_2/2\pi = 10$ GHz) determined solely by L_2, whereas ω_3 is a tunable value through the boundary condition of Port 3 at the SQUID. In figure 2(c), we show the dependence of ω_3 on the boundary condition under the parameter values in table 1. In the following part of this paper, we express the boundary condition at the end of Port 3 by the value of ω_3. For $L_3 = 4.5$ mm, $\omega_3/2\pi$ is tunable within the range from 4.567 GHz to 10.945 GHz.

3.2. Cavity mode

Next, we consider the eigenmodes whose amplitudes vanish in Port 1. For these modes, the field amplitude is localized in a finite region, Ports 2 and 3. We refer to such localized modes as the *cavity* modes in this study. Putting $\alpha_\omega^{(1)} = 0$ in equation (4), we immediately have $\cos(\omega L_2/v) = 0$ and $\cos(\omega L_{3,\omega}^{\text{eff}}/v) = 0$. This implies that such eigenmodes that are completely localized in a finite domain can exist under a specific boundary condition at the SQUID.

Regarding the lowest cavity mode, the condition for the existence of a completely localized mode is the exact tuning of ω_3 to ω_2. Its mode function is written as

$$\phi_{\text{cav}}(r) = \phi_0 \times \begin{cases} 0 & (\text{Port } 1) \\ -\sin(\omega_2 r_2/v) & (\text{Port } 2) \\ \sin(\omega_2 r_3/v) & (\text{Port } 3) \end{cases}, \tag{8}$$

where ϕ_0 is a constant. The spatial profile of this mode is schematically illustrated in figure 2(d).

When ω_3 is exactly tuned to ω_2, the cavity mode is completely decoupled from the propagating modes in Port 1. In other words, the external decay rate κ of the cavity mode to the waveguide modes is zero in this case. In contrast, when ω_3 is detuned slightly from ω_2, the cavity mode is weakly coupled from the propagating modes in Port 1, and κ takes a nonzero value. Then, the cavity mode becomes spectroscopically visible by the input microwave applied from Port 1, as we discuss in section 4.

3.3. General eigenmode

For a general frequency $[\cos(\omega L_2/v) \neq 0$ and $\cos(\omega L_{3,\omega}^{\text{eff}}/v) \neq 0]$, the eigenmode amplitudes do not vanish in all three ports. From equations (4) and (5), θ_ω, $\alpha_\omega^{(2)}/\alpha_\omega^{(1)}$ and $\alpha_\omega^{(3)}/\alpha_\omega^{(1)}$ are determined by the following equations,

$$\tan\theta_\omega = \tan(\omega L_2/v) + \tan\left(\omega L_{3,\omega}^{\text{eff}}/v\right), \tag{9}$$

$$\frac{\alpha_\omega^{(2)}}{\alpha_\omega^{(1)}} = \frac{\cos\theta_\omega}{\cos(\omega L_2/v)}, \tag{10}$$

$$\frac{\alpha_\omega^{(3)}}{\alpha_\omega^{(1)}} = \frac{\cos\theta_\omega}{\cos\left(\omega L_{3,\omega}^{\text{eff}}/v\right)}. \tag{11}$$

4. Spectroscopy of cavity mode

4.1. Phase shift upon reflection

Under a general boundary condition at the SQUID (where $\omega_3 \neq \omega_2$), the cavity mode (Ports 2 and 3) is coupled to the waveguide modes (Port 1) and responds to a microwave signal input through Port 1. In this subsection, we investigate the phase shift upon reflection of a stationary input field. From the eigenmode function in Port 1 [equation (1)], this phase shift is identified as $2\theta_\omega$, where θ_ω is determined by equation (9). This is plotted against the input frequency ω in figure 3(a) for two different boundary conditions at the SQUID. We observe an abrupt increase of the phase shift by 2π around a certain frequency ω_c and within a certain bandwidth κ. This fact supports that Ports 2 and 3 function as an effective cavity mode with the central frequency ω_c and the linewidth κ. We also observe that ω_c and κ are sensitive to the boundary condition, as we will discuss in detail in section 5.

4.2. Cavity photon energy

In this subsection, we investigate the photon energy stored in the cavity mode. We consider a stationary field at frequency ω whose waveform is given by $\phi(r,t) = \phi_\omega(r)\cos(\omega t)$, where $\phi_\omega(r)$ is the eigenmode function at frequency ω [equation (1)]. The energy density $\widetilde{E}$ per unit length of the waveguide is written as

$$\widetilde{E} = \frac{\widetilde{C}}{2}\left(\frac{\partial\phi}{\partial t}\right)^2 + \frac{1}{2\widetilde{L}}\left(\frac{\partial\phi}{\partial r}\right)^2, \tag{12}$$

where $\widetilde{C}$ and $\widetilde{L}$ respectively denote the capacitance and inductance per unit length, which are related to the microwave velocity v and the characteristic impedance Z of this waveguide by $\widetilde{C} = 1/(vZ)$ and $\widetilde{L} = Z/v$. Integrating the energy density $\widetilde{E}$ in the cavity part (Ports 2 and 3), the time-averaged photon energy E stored in the cavity is given by

$$E = \frac{\omega^2}{4vZ}\left[\left(\alpha_\omega^{(2)}\right)^2 L_2 + \left(\alpha_\omega^{(3)}\right)^2 L_3\right]. \tag{13}$$

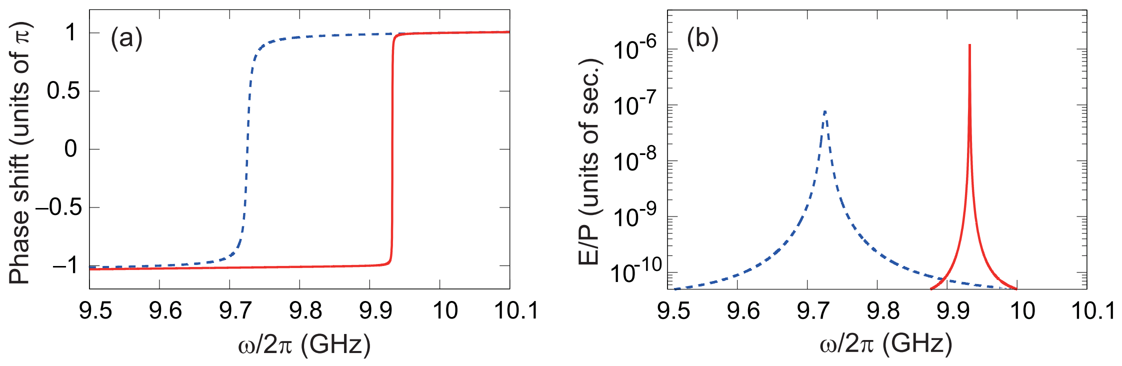

Figure 3. Spectroscopy of cavity mode. (a) Phase shift of the input field from Port 1 upon reflection and (b) cavity photon energy normalized by the input power, plotted against the input frequency ω. The boundary condition at the SQUID is set so that $\omega_3/2\pi = 9.6$ GHz (blue dotted) and 9.9 GHz (red solid).

Regarding the input field propagating in Port 1, it is identified from equation (1) as $(\alpha_\omega^{(1)}/2) \times \cos(\omega r_1/v + \omega t + \theta_\omega)$. Therefore, the time-averaged power $P(= v\widetilde{E})$ of the input field is given by $P = \omega^2(\alpha_\omega^{(1)})^2/8Z$. The cavity photon energy normalized by the input power is given by

$$E/P = \frac{2}{v}\left[\left(\alpha_\omega^{(2)}/\alpha_\omega^{(1)}\right)^2 L_2 + \left(\alpha_\omega^{(3)}/\alpha_\omega^{(1)}\right)^2 L_3\right], \tag{14}$$

which depends only on the input frequency ω and is insensitive to the field strength. In figure 3(b), we plot E/P evaluated by equation (14) against the input frequency ω. We observe a sharp peak around a certain frequency ω_c. This fact also supports that Ports 2 and 3 function as an effective cavity mode.

On the other hand, the standard quantum-optics theory predicts that, for a cavity with the central frequency ω_c and the linewidth κ, E/P has a Lorentzian shape as given by

$$E/P = \frac{\kappa}{(\omega - \omega_c)^2 + \kappa^2/4}. \tag{15}$$

We can confirm that the lineshape of E/P is a Lorentzian in agreement with equation (15).

5. Tuning of cavity parameters

5.1. Determination of cavity parameters

We can identify the resonance frequency ω_c and the linewidth κ of the cavity mode from the phase shift of a stationary input field upon reflection [figure 3(a)]. ω_c is identified as the frequency at which the phase shift becomes zero, whereas κ is identified as the difference in frequencies at which the phase shift becomes $\pm\pi/2$. Alternatively, we can determine ω_c and κ from the cavity photon energy normalized by the input power [figure 3(b)]. ω_c and κ are identified as the peak position and the linewidth of the Lorentzian, respectively. The resonance frequency ω_c and the linewidth κ thus determined are respectively plotted in figures 4(a) and (b), varying the boundary condition. We observe that the above two methods yield almost identical results.

5.2. Dependence of cavity parameters on boundary condition

As we observe in figure 4(a), the resonance frequency ω_c lies between ω_2 and ω_3 and exhibits an almost linear dependence on ω_3. In contrast, as we observe in figure 4(b), the linewidth κ depends drastically on the boundary condition. In particular, when ω_3 is tuned exactly to ω_2, the linewidth κ vanishes in principle. In this case, the cavity mode extending in Ports 2 and 3 has a node at the waveguide branch [figure 2(d)] and becomes completely decoupled from the propagating modes in Port 1. If the boundary condition is slightly varied from this state, the node position is shifted from the waveguide branch and coupling to the propagating modes in Port 1 is recovered.

When the detuning between ω_3 and ω_2 is large, in clear contrast with the case of small detuning, the cavity-waveguide coupling κ readily reaches the order of a gigahertz. The coupling is maximized when ω_3 is most detuned from ω_2, where $\kappa/2\pi$ reaches 1.25 GHz as we observe in figure 4(b). Such a large coupling is available because our setup contains no circuit element such as a capacitance that clearly divides the cavity and the waveguide and sets the upper limit on their coupling. Thus, the present device is equipped with an extremely wide tunability of the cavity-waveguide coupling.

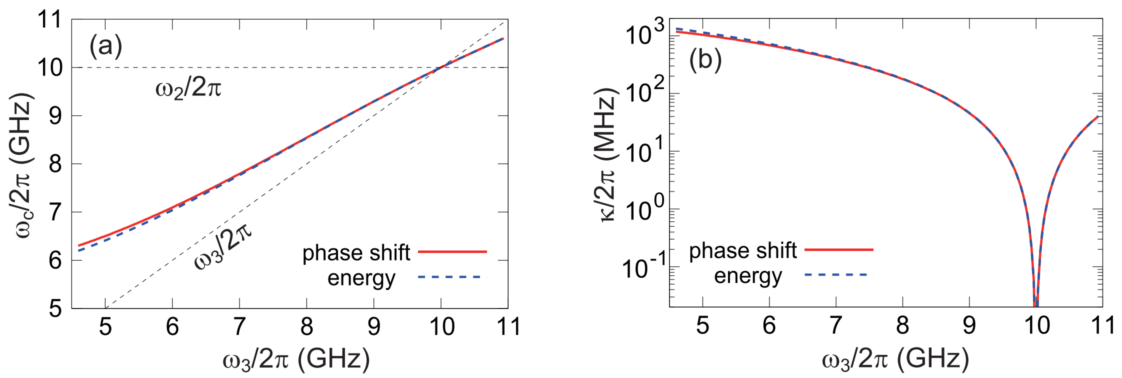

Figure 4. Dependences of (a) central frequency ω_c and (b) linewidth κ of the cavity mode, on the boundary condition at the SQUID. Red solid (blue dotted) lines plot the values estimated from the phase shift upon reflection (the cavity photon energy). In (a), ω_2 (fixed at $2\pi \times 10$ GHz) and ω_3 are also plotted by thin lines for reference.

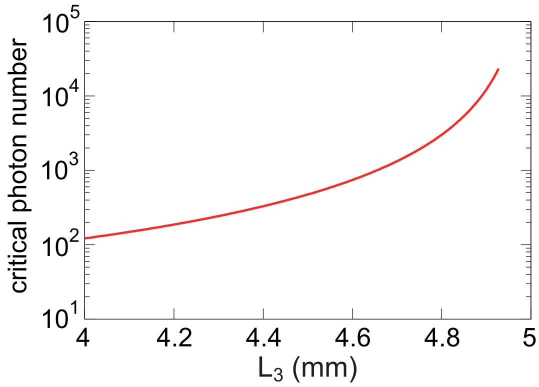

Figure 5. Critical photon number for the lowest cavity mode at 10 GHz. Note that tuning of $\omega_3/2\pi$ to 10 GHz is impossible under any boundary condition at the SQUID for $L_3 > 4.93$ mm.

5.3. Critical photon number

Since the present setup contains a Josephson junction at the end of Port 3, the cavity mode is expected to be nonlinear to some extent. The critical photon number is defined as the photon number above which the nonlinearity of this cavity gradually becomes apparent.

In this work, in derivation of the boundary condition at the SQUID (see appendix A), we employ a linear approximation $[\sin(2e\phi/\hbar) \approx 2e\phi/\hbar]$ to the flux field at the SQUID position. This requires that the flux there is sufficiently smaller than the magnetic flux quantum ($\hbar/2e$) and sets a critical photon number N_{crit} to the cavity. Considering the flux at the SQUID position [$r_3 = L_3$ in equation (8)], the condition for the linearization is written as

$$|\phi_0 \sin[\pi L_3/(2L_2)]| \lesssim \hbar/2e. \tag{16}$$

On the other hand, integrating equation (12) in Ports 2 and 3 and using $N = E/(\hbar\omega_2)$, the cavity photon number N is given by

$$N = \frac{\pi(1 + L_3/L_2)\phi_0^2}{4\hbar Z}. \tag{17}$$

From equations (16) and (17), the critical photon number is estimated to be

$$N_{\mathrm{crit}} \sim \frac{\pi\hbar(1 + L_3/L_2)}{16e^2 Z \sin^2(\pi L_3/2L_2)}. \tag{18}$$

In figure 5, we plot the critical photon number of the lowest cavity mode, varying the length L_3 of Port 3. The cavity mode amplitude at the SQUID position is proportional to $\sin(\omega_2 L_3/v)$ [equation (8)] and becomes smaller as L_3 approaches to 5 mm ($= \pi v/\omega_2$). As a result, the critical photon number increases in this limit. However, note that we cannot tune ω_3 to ω_2 for $L_3 > 4.93$ mm, as we observe in figure 2(c).

6. Discussion

We compare the performance metrics of the recent cavity-waveguide tunable couplers based on the DC SQUIDs [23–26] and the present one. In all these devices, the cavity-waveguide couplings are controlled through the DC currents near the SQUIDs. Therefore, the switching times of these devices are expected to be of the same order, a few nanoseconds [23]. The Josephson junctions forming the SQUIDs are the principal loss origin in these devices and determine the intrinsic cavity decay rates $\kappa_\mathrm{i}/2\pi$. These rates for the existent devices are around ten kilohertz [23, 26] and the proposed device would have a similar value. Regarding the range of the external cavity decay rates $\kappa_\mathrm{e}/2\pi$, the maximal values for the existent devices are around a few ten megahertz [23, 26], whereas that for the present device is expected to reach the gigahertz order as we observe in figure 4(b). The minimum external decay rates are by far lower than the intrinsic decay rates for the existent devices, and the same is expected also for the present device.

In contrast with the conventional cavity-waveguide systems coupled by capacitors or inductors, in the present galvanically-connected setup, the cavity (ports 2 and 3) and the waveguide (port 1) are strongly coupled by default. They become decoupled under a specific boundary condition at the SQUID, where ω_3 is set close to ω_2. As we observe in figure 4(b), the cavity linewidth is highly sensitive to ω_3 (and accordingly to the external flux threading the SQUID) around $\omega_3 \approx \omega_2$. This implies that the precise SQUID tuning is required not to achieve the ultrastrong cavity-waveguide coupling but to eliminate the coupling.

The present setup supports multiple cavity modes. As we discussed in section 3.1, their eigenfrequencies are given by $\omega = (\frac{1}{2}+n)\frac{\pi v}{L_2}$ $(n = 0, 1, \cdots)$, which are the solutions of $\cos(\omega L_2/v) = 0$. Since the mode separation is sufficiently large (20 GHz for $L_2 = 2.5$ mm), the existence of other cavity modes are negligible when investigating a certain cavity mode.

As an application of the present device, we discuss the conversion of a continuous wave to a ultrashort pulse. For this purpose, we capacitively couple another waveguide at the end of Port 2 as an input port of the continuous wave. The coupling strength is chosen so that the photon escape rate $\kappa_{\mathrm{e}2}$ from Port 2 to this waveguide becomes identical to the intrinsic loss rate κ_i of the cavity mode. At the storage stage, we turn off the coupling between the cavity mode and Port 1 ($\kappa_{\mathrm{e}1} = 0$) and apply a continuous wave resonant to the cavity with a photon rate of $|E_\mathrm{in}|^2$. Then, due to the critical coupling ($\kappa_{\mathrm{e}2} = \kappa_\mathrm{i}$), the average photon number stored in the cavity mode reaches $|E_\mathrm{in}|^2/\kappa_\mathrm{i}$ in the stationary state. At the emission stage, we turn on the cavity-Port 1 coupling ($\kappa_{\mathrm{e}1}/2\pi \sim 1$ GHz) and emit the stored photons to Port 1 as a short pulse. Since the output pulse length is of the order of $1/\kappa_{\mathrm{e}1}$, the output photon rate $|E_\mathrm{out}|^2$ is estimated by $|E_\mathrm{out}|^2/\kappa_{\mathrm{e}1} \sim |E_\mathrm{in}|^2/\kappa_\mathrm{i}$. Therefore, the instantaneous gain $|E_\mathrm{out}|^2/|E_\mathrm{in}|^2$ is roughly given by $\kappa_{\mathrm{e}1}/\kappa_\mathrm{i}$. For $\kappa_{\mathrm{e}1}/2\pi = 1$ GHz and $\kappa_\mathrm{i}/2\pi = 10$ kHz, the instantaneous gain reaches 50 dB. The upper bound of the input photon power is determined by the condition that the stationary cavity photon number is below the critical photon number [equation (18)], which is rewritten as $|E_\mathrm{i}|^2 \lesssim \kappa_\mathrm{i} N_\mathrm{crit}$. When the input field frequency is 10 GHz, the upper bound of the input power is -127 (-113) dBm for $L_3 = 4.5$ (4.9) mm.

7. Summary

In this study, we theoretically propose a galvanically connected cavity-waveguide tunable coupler. The investigated setup is a waveguide composed of three ports with the same property: one port is semi-infinite, whereas the other two ports have finite lengths. One of the finite ports is terminated by a SQUID and functions as a tunable stub. We analyzed the microwave response of this waveguide using its continuous eigenmodes and observed that this setup functions as a tunable cavity-waveguide coupler under an adequate choice of the lengths of the finite ports. The working principle of this tunable coupler is the shift of the node position of the cavity mode with respect to the waveguide branch. Due to the galvanic connection, this device is equipped with a very wide tunability of the cavity-waveguide coupling strength, which is applicable to the generation of an ultrashort microwave pulse for example.

Data availability statement

All data that support the findings of this study are included within the article (and any supplementary files).

Acknowledgments

The author is grateful to K Mizuno, Y Sunada, T Yamamoto, and K Semba for fruitful discussions. This work was supported by JST Moonshot R&D (JPMJMS2061, JPMJMS2067) and JSPS KAKENHI (22K03494).

Appendix A. Boundary condition at SQUID

As the SQUID terminating Port 3, we consider the one composed of two identical Josephson junctions (each having capacitance C_s and Josephson energy E_s) forming a loop. We denote the external magnetic flux threading the loop by $(\hbar/2e)\phi_{\mathrm{ex}}$. Then, after linearization $[\sin(2e\phi/\hbar) \approx 2e\phi/\hbar]$, the boundary condition at the SQUID position is written as [19]

$$\widetilde{C}_s \frac{\partial^2 \phi}{\partial t^2} = -\left(\frac{2e}{\hbar}\right)^2 \widetilde{E}_s(\phi_{\mathrm{ex}})\,\phi - \frac{1}{\widetilde{L}}\frac{\partial \phi}{\partial r}, \tag{A1}$$

where $\widetilde{C}_s = 2C_s$, $\widetilde{E}_s(\phi_{\mathrm{ex}}) = 2E_s|\cos(\phi_{\mathrm{ex}}/2)|$, and $\widetilde{L}(=Z/v)$ is the inductance of the waveguide per unit length. Putting $\phi(r,t) = \phi^{(3)}_\omega(r_3)\mathrm{e}^{-\mathrm{i}\omega t}$ in equation (A1), where $\phi^{(3)}_\omega(r_3)$ is given by equation (1), we obtain

$$\tan\left[\omega\left(L^{\mathrm{eff}}_{3,\omega} - L_3\right)/v\right] = 2ZC_s\omega - \frac{8e^2 Z E_s}{\hbar^2\omega}|\cos(\phi_{\mathrm{ex}}/2)|. \tag{A2}$$

This is an equation to determine $L^{\mathrm{eff}}_{3,\omega}$ for a given frequency ω.

Putting $\omega = \omega_3$ in equation (A2) and using equation (7), we obtain

$$\cot(\omega_3 L_3/v) = 2ZC_s\omega_3 - \frac{8e^2 Z E_s}{\hbar^2\omega_3}|\cos(\phi_{\mathrm{ex}}/2)|. \tag{A3}$$

This is an equation to determine ω_3. The numerical solution of this equation is shown in figure 2(c) in the main text.

Appendix B. Boundary condition at waveguide branch

Here, we derive the boundary condition at a waveguide branch from the circuit model having three ports A, B, and C (figure B1). The classical Lagrangian describing this circuit is given by

$$\begin{aligned} L = &\frac{\Delta C}{2}\dot{\phi}_0^2 - \frac{1}{2\Delta L}\left[(\phi_0-\phi_{a1})^2 + (\phi_0-\phi_{b1})^2 + (\phi_0-\phi_{c1})^2\right] \\ &+ \frac{\Delta C}{2}\left[\dot{\phi}_{a1}^2 + \dot{\phi}_{b1}^2 + \dot{\phi}_{c1}^2\right] - \frac{1}{2\Delta L}\left[(\phi_{a1}-\phi_{a2})^2 + (\phi_{b1}-\phi_{b2})^2 + (\phi_{c1}-\phi_{c2})^2\right] \\ &+ \cdots. \end{aligned} \tag{B1}$$

From this Lagrangian, we can derive the equation of motion for the flux ϕ_0 at the branch point,

$$\Delta C\ddot{\phi}_0 = \left[(\phi_{a1}-\phi_0) + (\phi_{b1}-\phi_0) + (\phi_{c1}-\phi_0)\right]/\Delta L. \tag{B2}$$

We here switch to the continuous description of the flux field, namely, $\phi_{aj}(t) = \phi_a(j\Delta r, t)$, where Δr is the infinitesimal distance between the nodes. $\phi_b(r_b,t)$ and $\phi_c(r_c,t)$ are introduced similarly. Since the flux ϕ_0 is common to the three semi-infinite waveguides, we immediately have

$$\phi_a(0,t) = \phi_b(0,t) = \phi_c(0,t). \tag{B3}$$

With the continuous description, equation (B2) is rewritten as

$$\Delta C\frac{\partial^2\phi_a}{\partial t^2}(0,t) = \frac{1}{\widetilde{L}}\left[\frac{\partial\phi_a}{\partial r_a}(0,t) + \frac{\partial\phi_b}{\partial r_b}(0,t) + \frac{\partial\phi_c}{\partial r_c}(0,t)\right], \tag{B4}$$

where $\widetilde{L} = \Delta L/\Delta r$ is the inductance per unit length. Since the left-hand side of equation (B4) is proportional to ΔC and is therefore infinitesimal, we obtain

$$\frac{\partial\phi_a}{\partial r_a}(0,t) + \frac{\partial\phi_b}{\partial r_b}(0,t) + \frac{\partial\phi_c}{\partial r_c}(0,t) = 0. \tag{B5}$$

Equations (B3) and (B5) are the boundary conditions at the waveguide branch.

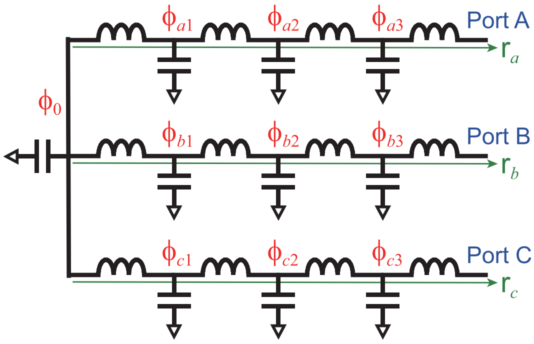

Figure B1. Circuit diagram of a waveguide branch. All capacitors (inductors) have infinitesimal capacitance ΔC (inductance ΔL).

ORCID iD

Kazuki Koshino https://orcid.org/0000-0002-9754-4463

References

[1] Walther H, Varcoe B T H, Englert B-G and Becker T 2006 Cavity quantum electrodynamics *Rep. Prog. Phys.* **69** 1325
[2] Blais A, Grimsmo A L, Girvin S M and Wallraff A 2021 Circuit quantum electrodynamics *Rev. Mod. Phys.* **93** 025005
[3] Kockum A F, Miranowicz A, De Liberato S, Savasta S and Nori F 2019 Ultrastrong coupling between light and matter *Nat. Rev. Phys.* **1** 19
[4] Forn-Diaz P, Lamata L, Rico E, Kono J and Solano E 2019 Ultrastrong coupling regimes of light-matter interaction *Rev. Mod. Phys.* **91** 025005
[5] Wallquist M, Shumeiko V S and Wendin G 2006 Selective coupling of superconducting charge qubits mediated by a tunable stripline cavity *Phys. Rev.* B **74** 224506
[6] DiCarlo L *textitet al* 2009 Demonstration of two-qubit algorithms with a superconducting quantum processor *Nature* **460** 240
[7] Barends R *et al* 2014 Superconducting quantum circuits at the surface code threshold for fault tolerance *Nature* **508** 500
[8] Kelly J *et al* 2015 State preservation by repetitive error detection in a superconducting quantum circuit *Nature* **519** 66
[9] Yan F, Krantz P, Sung Y, Kjaergaard M, Campbell D L, Orlando T P, Gustavsson S and Oliver W D 2018 Tunable coupling scheme for implementing high-fidelity two-qubit gates *Phys. Rev. Appl.* **10** 054062
[10] Niskanen A O, Harrabi K, Yoshihara F, Nakamura Y, Lloyd S and Tsai J S 2007 Quantum coherent tunable coupling of superconducting qubits *Science* **316** 723
[11] Chen Y *et al* 2014 Qubit architecture with high coherence and fast tunable coupling *Phys. Rev. Lett.* **113** 220502
[12] Kounalakis M, Dickel C, Bruno A, Langford N K and Steele G A 2018 Tuneable hopping and nonlinear cross-Kerr interactions in a high-coherence superconducting circuit *npj Quantum Inf.* **4** 38
[13] Goto H 2022 Double-transmon coupler: fast two-qubit gate with no residual coupling for highly detuned superconducting qubits *Phys. Rev. Appl.* **18** 034038
[14] Campbell D L, Kamal A, Ranzani L, Senatore M and LaHaye M D 2023 Modular tunable coupler for superconducting circuits *Phys. Rev. Appl.* **19** 064043
[15] Zhang H *et al* 2024 Tunable inductive coupler for high-fidelity gates between fluxonium qubits *PRX Quantum* **5** 020326
[16] Baust A *et al* 2015 Tunable and switchable coupling between two superconducting resonators *Phys. Rev.* B **91** 014515
[17] Wulschner F *et al* 2016 Tunable coupling of transmission-line microwave resonators mediated by an rf SQUID *EPJ Quantum Technol.* **3** 10
[18] Miyanaga T, Tomonaga A, Ito H, Mukai H and Tsai J S 2021 Ultrastrong tunable coupler between superconducting LC resonators *Phys. Rev. Appl.* **16** 064041
[19] Koshino K and Nakamura Y 2012 Control of the radiative level shift and linewidth of a superconducting artificial atom through a variable boundary condition *New J. Phys.* **14** 043005
[20] Forn-Diaz P, Warren C W, Chang C W S, Vadiraj A M and Wilson C M 2017 On-demand microwave generator of shaped single photons *Phys. Rev. Appl.* **8** 054015
[21] Kurpiers P *et al* 2018 Deterministic quantum state transfer and remote entanglement using microwave photons *Nature* **558** 264
[22] Janzen N, Dai X, Ren S, Shi J and Lupascu A 2023 Tunable coupler for mediating interactions between a two-level system and a waveguide from a decoupled state to the ultrastrong coupling regime *Phys. Rev. Res.* **5** 033155
[23] Yin Y *et al* 2013 Catch and release of microwave photon states *Phys. Rev. Lett.* **110** 107001
[24] Sete E A, Galiautdinov A, Mlinar E, Martinis J M and Korotkov A N 2013 Catch-disperse-release readout for superconducting qubits *Phys. Rev. Lett.* **110** 210501
[25] Pierre M, Svensson I-M, Sathyamoorthy S R, Johansson G and Delsing P 2014 Storage and on-demand release of microwaves using superconducting resonators with tunable coupling *Appl. Phys. Lett.* **104** 232604
[26] Pierre M, Sathyamoorthy S R, Svensson I-M, Johansson G and Delsing P 2019 Resonant and off-resonant microwave signal manipulation in coupled superconducting resonators *Phys. Rev.* B **99** 094518
[27] Bockstiegel C, Wang Y, Vissers M R, Wei L F, Chaudhuri S, Hubmayr J and Gao J 2016 A tunable coupler for superconducting microwave resonators using a nonlinear kinetic inductance transmission line *Appl. Phys. Lett.* **108** 222604